

Impact of the electron-electron correlation on phonon dispersion: Failure of LDA and GGA DFT functionals in graphene and graphite

Michele Lazzeri,¹ Claudio Attaccalite,² Ludger Wirtz,³ and Francesco Mauri¹

¹IMPMC, Universités Paris 6 et 7, IPGP, CNRS, 140 rue de Lourmel, 75015 Paris, France

²Unidad de Física de Materiales, European Theoretical Spectroscopy Facility (ETSF), Universidad del País Vasco, 20018 San Sebastian, Spain

³Institute for Electronics, Microelectronics, and Nanotechnology, CNRS, 59652 Villeneuve d'Ascq, France

(Received 29 May 2008; published 26 August 2008)

We compute the electron-phonon coupling (EPC) of selected phonon modes in graphene and graphite using various *ab initio* methods. The inclusion of nonlocal exchange-correlation effects within the *GW* approach strongly renormalizes the square EPC of the A_1' \mathbf{K} mode by almost 80% with respect to density-functional theory in the LDA and GGA approximations. Within *GW*, the phonon slope of the A_1' \mathbf{K} mode is almost two times larger than in GGA and LDA, in agreement with phonon dispersions from inelastic x-ray scattering and Raman spectroscopy. The hybrid B3LYP functional overestimates the EPC at \mathbf{K} by about 30%. Within the Hartree-Fock approximation, the graphene structure displays an instability under a distortion following the A_1' phonon at \mathbf{K} .

DOI: 10.1103/PhysRevB.78.081406

PACS number(s): 78.30.Na, 71.15.Mb, 63.20.kd, 81.05.Uw

The electron-phonon coupling (EPC) is one of the fundamental quantities in condensed matter. It determines phonon dispersions and Kohn anomalies, phonon-mediated superconductivity, electrical resistivity, Jahn-Teller distortions, etc. Nowadays, density-functional theory (DFT) within local and semilocal approximations is considered the “standard model” to compute *ab initio* the electron-phonon interaction and phonon dispersions.¹ Thus, a failure of DFT would have major consequences in a broad context. In GGA and LDA approximations,² the electron exchange-correlation energy is a local functional of the charge density, and the long-range character of the electron-electron interaction is neglected. These effects are taken into account by Green's-function approaches based on the screened electron-electron interaction W such as the *GW* method.³ *GW* is considered the most precise *ab initio* approach to determine electronic bands, but so far it has never been used to compute EPCs nor phonon dispersions. The semiempirical B3LYP functional² partially includes long-range Hartree-Fock (HF) exchange. B3LYP has been used to compute phonon frequencies but, so far, not the EPC.

The EPC is a key quantity for graphene, graphite, and carbon nanotubes. It determines the Raman spectrum, which is the most common characterization technique for graphene and nanotubes^{4,5} and the high-bias electron transport in nanotubes.⁶ Graphene and graphite are quite unique systems in which the actual value of the EPC for some phonons can be obtained almost directly from measurements. In particular, the square of the EPC of the highest optical-phonon branch (HOB) at the symmetry \mathbf{K} point is proportional to the HOB slope near \mathbf{K} .⁷ The HOB \mathbf{K} slope can be measured by inelastic x-ray scattering (IXS)^{8,9} or by the dispersion of the D and 2D lines as a function of the excitation energy in a Raman experiment.^{5,10–13} A careful look at the most recent data suggests that the experimental phonon slopes (and thus the EPC) are underestimated by DFT.⁵ The ability of DFT (LDA and GGA) in describing the EPC of graphene was also questioned by a recent theoretical work.¹⁴

Here, we show that: (i) the *GW* approach, which provides the most accurate *ab initio* treatment of electron correlation, can be used to compute the electron-phonon interaction and the phonon dispersion; (ii) in graphite and graphene, DFT (LDA and GGA) underestimates, by a factor of 2, the slope

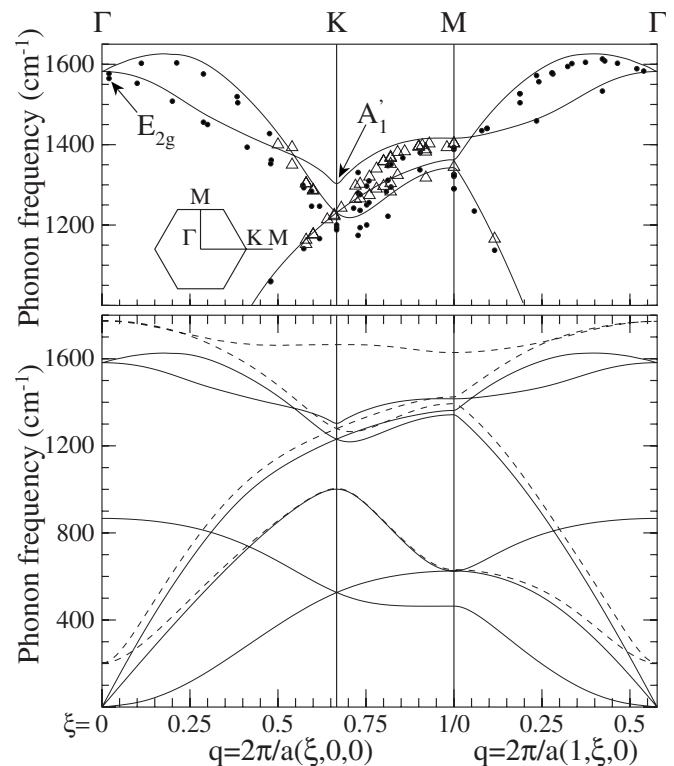


FIG. 1. Upper panel: Phonon dispersion of graphite. Lines are DFT calculations, dots and triangles are IXS measurements from Refs. 8 and 9, respectively. Lower panel: Phonon dispersion of graphene from DFT calculations. Dashed lines are obtained by subtracting, from the dynamical matrix, the phonon self-energy between the π bands (ω_q in the text).

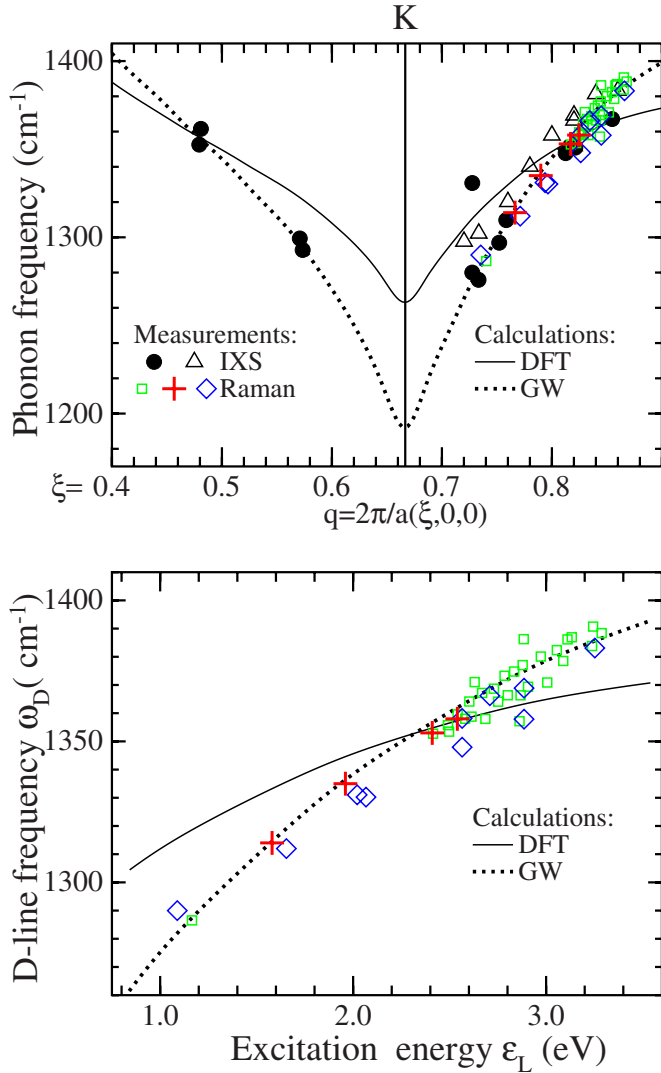


FIG. 2. (Color online). Upper panel: Dispersion of the highest optical phonon in graphite near \mathbf{K} . Calculations are from DFT or corrected to include GW renormalization of the EPC. Here, the DFT dispersion is vertically shifted by -40 cm^{-1} to fit measurements. Dots and triangles are IXS data from Refs. 8 and 9, respectively. Squares, plus, and diamonds are obtained from Raman data of Refs. 10–12, respectively, using the double-resonance model (Refs. 12 and 13). Lower panel: Dispersion of the Raman D line.

of the phonon dispersion of the highest optical branch at the zone boundary and the square of its EPC by almost 80%; (iii) GW reproduces the experimental phonon dispersion near \mathbf{K} , the value of the EPC, and the electronic band dispersion; (iv) the B3LYP hybrid functional² gives phonons close to GW but overestimates the EPC at \mathbf{K} by about 30%; and (v) within HF the graphite structure is unstable.

In Fig. 1, we show the phonon dispersion of graphite computed with DFT_{GGA}.¹⁵ In spite of the general good agreement with IXS data, the situation is not clear for the HOB near \mathbf{K} . In fact, despite the scattering among experimental data, the theoretical HOB is always higher in energy with respect to measurements, and the theoretical phonon slope (for the HOB near \mathbf{K}) is underestimating the measured one. It is also remarkable that while the DFT \mathbf{K} frequency is

$\sim 1300 \text{ cm}^{-1}$, the highest measured is much lower at $\sim 1200 \text{ cm}^{-1}$.

The dispersion of the HOB near \mathbf{K} can also be obtained by Raman measurements of the graphene and graphite D line ($\sim 1350 \text{ cm}^{-1}$).¹² The D-line frequency ω_D depends on the energy of the exciting laser ϵ_L . According to the double-resonance model,^{12,13} ϵ_L activates a phonon of the HOB with momentum $\mathbf{q}=\mathbf{K}+2\Delta\mathbf{q}$ along the \mathbf{K} -M line⁵ and energy $\hbar\omega_D$. $\Delta\mathbf{q}$ is determined by $\epsilon_{\mathbf{K}-\Delta\mathbf{q},\pi^*}-\epsilon_{\mathbf{K}-\Delta\mathbf{q},\pi}=\epsilon_L-\hbar\omega_D/2$ where $\epsilon_{\mathbf{k},\pi/\pi^*}$ is the energy of the π/π^* electronic state with momentum \mathbf{k} . Thus, by measuring ω_D vs ϵ_L and considering the electronic π bands dispersion from DFT, one can obtain the phonon dispersion ω_D vs \mathbf{q} .¹² The phonon dispersion thus obtained is very similar to the one from IXS data and its slope is clearly underestimated by DFT (Fig. 2, upper panel). The same conclusion is reached by comparing the D-line dispersion ω_D vs ϵ_L (directly obtained from measurements) with calculations (Fig. 2, lower panel). Note that the dispersions of the Raman 2D line⁵ is consistent with that of the D line and thus in disagreement with DFT (LDA and GGA) as well.

The steep slope of the HOB near \mathbf{K} is due to the presence of a Kohn anomaly for this phonon.⁷ In particular, in Ref. 7, it was shown that the HOB slope is entirely determined by the contribution of the phonon self-energy between π bands ($P_{\mathbf{q}}$) to the dynamical matrix $\mathcal{D}_{\mathbf{q}}$. $\omega_{\mathbf{q}}=\sqrt{\mathcal{D}_{\mathbf{q}}/m}$ is the phonon pulsation, where m is the mass. For a given phonon with momentum \mathbf{q} ,

$$\mathcal{D}_{\mathbf{q}}=B_{\mathbf{q}}+P_{\mathbf{q}}, \quad P_{\mathbf{q}}=\frac{4}{N_k} \sum_{\mathbf{k}} \frac{|D_{(\mathbf{k}+\mathbf{q})\pi^*,\mathbf{k}\pi}|^2}{\epsilon_{\mathbf{k},\pi}-\epsilon_{\mathbf{k}+\mathbf{q},\pi^*}}, \quad (1)$$

where the sum is performed on N_k wave vectors all over the Brillouin zone; $D_{(\mathbf{k}+\mathbf{q})i,\mathbf{k}j}=\langle \mathbf{k}+\mathbf{q},i|\Delta V_{\mathbf{q}}|\mathbf{k},j\rangle$ is the EPC; $\Delta V_{\mathbf{q}}$ is the derivative of the Kohn-Sham potential with respect to the phonon mode; and $|\mathbf{k},i\rangle$ is the Bloch eigenstate with momentum \mathbf{k} , band index i , and energy $\epsilon_{\mathbf{k},i}$. $\pi(\pi^*)$ identifies the occupied (empty) π band. In Fig. 1 we show a fictitious phonon dispersion $\tilde{\omega}_{\mathbf{q}}$ obtained by subtracting $P_{\mathbf{q}}$ from the dynamical matrix ($\omega_{\mathbf{q}}=\sqrt{B_{\mathbf{q}}/m}$) for each phonon. The HOB is the branch which is mostly affected and, for the HOB, $\omega_{\mathbf{q}}$ becomes almost flat near \mathbf{K} . Thus, DFT (LDA or GGA) fails in describing the HOB slope near \mathbf{K} , the slope which is determined by $P_{\mathbf{q}}$. $P_{\mathbf{q}}$ is given by the square of EPC divided by π -band energies. Thus, the DFT failure can be attributed to a poor description of the EPC or of the π -band dispersion.

In graphene and graphite, it is known that standard DFT provides an underestimation of the π - and π^* -band slopes of ~ 10 –20%.^{16,17} A very precise description of the bands, in better agreement with measurements, is obtained using GW.^{16,17} We thus computed the π bands with DFT (both LDA and GGA)¹⁸ and GW (Ref. 19) and compared with HF (Ref. 20) and B3LYP.²⁰ Details are in Ref. 21. The different methods provide band dispersions whose overall behavior can be described by a scaling of the π energies.¹⁶ The different scaling factors can be obtained by comparing $\Delta\epsilon_g$, the energy difference between the π^* and π bands at the symmetry point \mathbf{M} (\mathbf{L}) for graphene (graphite). $\Delta\epsilon_g$ is larger in

TABLE I. EPC of the Γ - E_{2g} and \mathbf{K} - A'_1 phonons computed with various approximations. $\Delta\epsilon_g$ (eV), $\langle D_{\mathbf{q}}^2 \rangle_F$ (eV $^2/\text{\AA}^2$), and $\alpha_{\mathbf{q}}$ (eV/ \AA^2) are defined in the text. ω_{Γ} ($\omega_{\mathbf{K}}$) is the phonon frequency of the E_{2g} A'_1 mode (cm $^{-1}$). The GW $\omega_{\mathbf{K}}$ for graphite (in parenthesis) is not computed directly (see the text). $i = \sqrt{-1}$ is the imaginary unit.

	Graphene						
	$\Delta\epsilon_g$	$\langle D_{\mathbf{q}}^2 \rangle_F$	α_{Γ}	ω_{Γ}	$\langle D_{\mathbf{K}}^2 \rangle_F$	$\alpha_{\mathbf{K}}$	$\omega_{\mathbf{K}}$
DFT _{LDA}	4.03	44.4	11.0	1568	89.9	22.3	1275
DFT _{GGA}	4.08	45.4	11.1	1583	92.0	22.5	1303
GW	4.89	62.8	12.8	–	193	39.5	–
B3LYP	6.14	82.3	13.4	1588	256	41.7	1172
HF	12.1	321	26.6	1705	6020	498	960 \times i
	Graphite						
	$\Delta\epsilon_g$	$\langle D_{\mathbf{q}}^2 \rangle_F$	α_{Γ}	ω_{Γ}	$\langle D_{\mathbf{K}}^2 \rangle_F$	$\alpha_{\mathbf{K}}$	$\omega_{\mathbf{K}}$
DFT _{LDA}	4.06	43.6	10.7	1568	88.9	21.8	1299
DFT _{GGA}	4.07	44.9	11.0	1581	91.5	22.5	1319
GW	4.57	58.6	12.8	–	164.2	35.9	(1192)

GW than in DFT (Table I). Thus, inclusion of the GW correction to the electronic bands alone results in a larger denominator in Eq. (1), providing a smaller phonon slope and a worse agreement with experiments. The underestimation of the \mathbf{K} phonon slope in DFT is thus due to the EPC.

The EPC can be computed with linear response as, e.g., in Ref. 7 but, at present, the use of this technique within GW is not feasible. Alternatively, the EPC associated with a phonon mode can be determined by the variation of the electronic band energies by displacing the atoms according to the considered mode. In graphene, at \mathbf{K} , there are doubly degenerate π electronic states at the Fermi level. The HOB corresponds to the E_{2g} phonon at Γ and to the A'_1 at \mathbf{K} . As an example, we consider the EPC associated with the Γ - E_{2g} phonon and we displace the atoms according to its phonon pattern (see Fig. 3). Following symmetry arguments,²² one can show that, in an arbitrary base of the two-dimensional space of the π bands at \mathbf{K} , the Hamiltonian is the 2×2 matrix

$$H = 2\sqrt{\langle D_{\mathbf{q}}^2 \rangle_F} \begin{pmatrix} a & b \\ b^* & -a \end{pmatrix} d + \mathcal{O}(d^2), \quad (2)$$

where each atom is displaced by d , $|a|^2 + |b|^2 = 1$, and $\langle D_{\mathbf{q}}^2 \rangle_F = \sum_{i,j}^{\pi,\pi^*} |D_{\mathbf{K}i,\mathbf{K}j}|^2/4$, where the sum is performed on the two degenerate π bands. Diagonalizing Eq. (2), we see that an atomic displacement following the Γ - E_{2g} phonon induces the splitting $\Delta E_{\Gamma} = \epsilon_{\mathbf{K},\pi^*} - \epsilon_{\mathbf{K},\pi}$ and

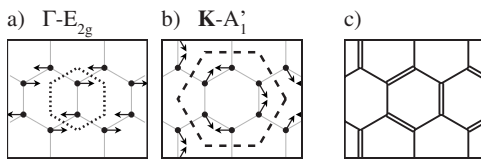


FIG. 3. (a) and (b) Patterns of the Γ - E_{2g} and \mathbf{K} - A'_1 phonons of graphene. Dotted and dashed lines are the Wigner-Seitz cells of the unit cell and of the $\sqrt{3} \times \sqrt{3}$ supercell. (c) HF equilibrium structure.

$$\langle D_{\mathbf{q}}^2 \rangle_F = \lim_{d \rightarrow 0} \frac{1}{16} \left(\frac{\Delta E_{\Gamma}}{d} \right)^2. \quad (3)$$

In analogous way, we define $\langle D_{\mathbf{K}}^2 \rangle_F = \sum_{i,j}^{\pi,\pi^*} |D_{(2\mathbf{K})i,\mathbf{K}j}|^2/4$ for the A'_1 phonon at \mathbf{K} . Let us consider a $\sqrt{3} \times \sqrt{3}$ graphene supercell. Such a cell can be used to displace the atoms following the \mathbf{K} - A'_1 phonon (Fig. 3) since the \mathbf{K} point is refolded in Γ . Let us call $\Delta E_{\mathbf{K}}$ the splitting of the $\epsilon_{\mathbf{K},\pi}$ bands induced by this displacement (since \mathbf{K} is refolded in Γ , here $\epsilon_{\mathbf{K},\pi}$ denotes the energies of the Γ band of the supercell corresponding to the π band at \mathbf{K} in the unit cell). Considering the atomic distortion of Fig. 3 and displacing each atom by d , one can show that

$$\langle D_{\mathbf{K}}^2 \rangle_F = \lim_{d \rightarrow 0} \frac{1}{8} \left(\frac{\Delta E_{\mathbf{K}}}{d} \right)^2. \quad (4)$$

In practice, by calculating band energies in the distorted structures of Fig. 3 and using Eqs. (3) and (4), one obtains the EPCs of the Γ - E_{2g} and \mathbf{K} - A'_1 phonons between π states. Similar equations can be used for graphite.²³ Results are in Table I together with the computed phonon frequencies. The EPCs from DFT_{GGA} are in agreement with those from linear response.⁷ We also remark that, within the present “frozen-phonon” approach, the Coulomb vertex corrections are implicitly included within GW .

To study the effect of the different computational methods on the phonon slope (which is determined by $P_{\mathbf{q}}$) we recall that $P_{\mathbf{q}}$ is the ratio of the square EPC and band energies [Eq. (1)]. Thus, we have to compare $\alpha_{\mathbf{q}} = \langle D_{\mathbf{q}}^2 \rangle_F / \Delta\epsilon_g$. As an example, assuming that the change in $P_{\mathbf{q}}$ from DFT to GW is constant for \mathbf{q} near \mathbf{K} ,

$$\frac{P_{\mathbf{q}}^{GW}}{P_{\mathbf{q}}^{DFT}} \approx \frac{\alpha_{\mathbf{K}}^{GW}}{\alpha_{\mathbf{K}}^{DFT}} = r^{GW} \quad (5)$$

and r^{GW} provides the change in the \mathbf{K} phonon slope going from DFT to GW . To understand the results, we recall that in standard DFT the exchange-correlation depends only on the local electron density. In contrast, the exchange interaction in HF and GW is nonlocal. Furthermore, in GW , correlation effects are nonlocal since they are described through a dynamically screened Coulomb interaction. The hybrid functional B3LYP gives results intermediate between DFT and HF.

Both α_{Γ} and $\alpha_{\mathbf{K}}$ are heavily overestimated by HF, the \mathbf{K} -EPC being so huge that graphene is no more stable (the $\mathbf{K}A'_1$ phonon frequency is not real). Indeed, the HF equilibrium geometry is a $\sqrt{3} \times \sqrt{3}$ reconstruction with alternating double and single bonds of 1.40 and 1.43 \AA lengths as in Fig. 3 (with a gain of 0.9 meV/atom). These results not only demonstrate the major effect of the long-range character of the exchange for the \mathbf{K} -EPC (Ref. 14) but also the importance of the proper inclusion of the screening (included in GW but neglected in HF). Notice also that $\alpha_{\mathbf{K}}^{GW}$ of graphite is smaller with respect to graphene by $\sim 10\%$. This is explained by the larger screening of the exchange in graphite (due to the presence of adjacent layers) than in graphene. On the contrary, within GGA and LDA, the graphite phonon frequencies and EPCs are very similar to those of graphene

since these functionals do not take into account the electron-electron interaction screening.

Concerning the phonon slope, α_{Γ}^{GW} is only 15% larger than α_{Γ}^{DFT} . Indeed, DFT reproduces with this precision the phonon frequency and dispersion of the HOB at Γ . On the contrary, $\alpha_{\mathbf{K}}^{GW}$ is 60% larger than $\alpha_{\mathbf{K}}^{DFT}$ for graphite. This large increase with respect to DFT could explain the disagreement between DFT and the measured A_1' phonon dispersion near \mathbf{K} . To test this, we need to determine the GW phonon dispersion that, using Eq. (5), becomes $\omega_{\mathbf{q}}^{GW} \simeq \sqrt{(B_{\mathbf{q}}^{GW} + r^{GW} P_{\mathbf{q}}^{DFT})}/m$, where $r^{GW}=1.6$. Moreover, we can assume $B_{\mathbf{q}}^{GW} \simeq B_{\mathbf{K}}^{GW}$ since the $B_{\mathbf{q}}$ component of the dynamical matrix [Eq. (1)] is not expected to have an important dependence on \mathbf{q} (Fig. 1). The value of $B_{\mathbf{K}}^{GW}$ is obtained as a fit to the measurements of Fig. 2.²⁴ The resulting $\mathbf{K} A_1'$ phonon frequency is 1192 cm^{-1} , which is our best estimation and is almost 100 cm^{-1} smaller than in DFT. The phonon dispersion thus obtained and the corresponding D-line dispersion are both in better agreement with measurements (Fig. 2).

The partial inclusion of long-range exchange within the semiempirical B3LYP functional leads to a strong increase in the EPC at \mathbf{K} as compared to the LDA and GGA functionals. However, comparing to the GW value, the EPC is overesti-

mated by 30% and the corresponding frequency for the $\mathbf{K}-A_1'$ mode at 1172 cm^{-1} falls well below the degenerate \mathbf{K} mode, which is around 1200 cm^{-1} in the experiment^{8,9} (Fig. 1) and at 1228 cm^{-1} in our phonon calculation with B3LYP. We have checked that tuning the percentage of HF exchange in the hybrid functional allows to match the EPC value of the GW approach (in which case, the $\mathbf{K}-A_1'$ mode remains the highest mode). This may be a good way to calculate the full phonon dispersion of graphite/graphene within DFT, yet with an accuracy close to the one of the GW approach.

Concluding, GW is a general approach to compute accurate EPC where DFT functionals fail. Such a failure in graphite/graphene is due to the interplay between the two-dimensional Dirac-type band structure and the long-range character of the Coulomb interaction.¹⁴ However, GW can be also used in cases (in which the EPC is badly described by DFT) where the electron exchange and correlation are more short ranged.²⁵

Calculations were done at IDRIS (Projects No. 081202 and No. 081827). C.A. and L.W. acknowledge French ANR Project No. PJC05_6741. We thank D. M. Basko, A. Rubio, J. Schamps, and C. Brouder for the discussions and A. Marini for the code YAMBO.

¹S. Baroni *et al.*, Rev. Mod. Phys. **73**, 515 (2001).

²LDA, GGA and B3LYP refer, respectively, to D. M. Ceperley *et al.*, Phys. Rev. Lett. **45**, 566 (1980); J. P. Perdew *et al.*, *ibid.* **77**, 3865 (1996); A. D. Becke, J. Chem. Phys. **98**, 5648 (1993).

³F. Aryasetiawan *et al.*, Rep. Prog. Phys. **61**, 237 (1998); W. G. Aulbur *et al.*, Solid State Phys. **54**, 1 (2000); G. Onida *et al.*, Rev. Mod. Phys. **74**, 601 (2002).

⁴S. Reich *et al.*, Philos. Trans. R. Soc. London, Ser. A **362**, 2271 (2004).

⁵A. C. Ferrari *et al.*, Phys. Rev. Lett. **97**, 187401 (2006); D. Graf *et al.*, Nano Lett. **7**, 238 (2007).

⁶Z. Yao *et al.*, Phys. Rev. Lett. **84**, 2941 (2000).

⁷S. Piscanec *et al.*, Phys. Rev. Lett. **93**, 185503 (2004).

⁸J. Maultzsch *et al.*, Phys. Rev. Lett. **92**, 075501 (2004).

⁹M. Mohr *et al.*, Phys. Rev. B **76**, 035439 (2007).

¹⁰I. Pócsik *et al.*, J. Non-Cryst. Solids **227**, 1083 (1998).

¹¹P. H. Tan *et al.*, Phys. Rev. B **66**, 245410 (2002).

¹²J. Maultzsch *et al.*, Phys. Rev. B **70**, 155403 (2004).

¹³C. Thomsen *et al.*, Phys. Rev. Lett. **85**, 5214 (2000).

¹⁴D. M. Basko *et al.*, Phys. Rev. B **77**, 041409(R) (2008).

¹⁵Calculations were done as in Ref. 1. Technical details and thus phonon dispersions are the same as in Ref. 7.

¹⁶S. Y. Zhou *et al.*, Phys. Rev. B **71**, 161403(R) (2005); S. G. Louie, in *Topics in Computational Materials Science*, editor by C. Y. Fong (World Scientific, Singapore, 1997), p. 96.

¹⁷A. Grüneis *et al.*, Phys. Rev. Lett. **100**, 037601 (2008).

¹⁸LDA and GGA calculations were done with the code PWSCF (<http://www.quantum-espresso.org>), with pseudopotentials of the type; N. Troullier *et al.*, Phys. Rev. B **43**, 1993 (1991).

¹⁹ GW calculations were done with the code YAMBO (the YAMBO project, <http://www.yambo-code.org/>), within the nonself-consistent G_0W_0 approximation starting from DFT-LDA wave functions and using a plasmon-pole model for the screening,

following; M. S. Hybertsen *et al.*, Phys. Rev. B **34**, 5390 (1986).

²⁰HF and B3LYP calculations were done with the code CRYSTAL (V. R. Saunders *et al.*, *CRYSTAL03 Users Manual* (University of Torino, Torino, 2003), using the TZ basis by Dunning (without the diffuse P function).

²¹For graphite we used the experimental lattice parameters ($a=2.46$ Å, $c=6.708$ Å). For graphene we used $a=2.46$ Å and a vacuum layer of 20 a.u. EPCs were calculated on a structure distorted by $d=0.01$ a.u. For graphene, the electronic integration on the 1×1 cell was done with a $18 \times 18 \times 1$ grid for LDA/GGA, $36 \times 36 \times 1$ for GW, and $66 \times 66 \times 1$ for B3LYP/HF. For graphite it was $18 \times 18 \times 6$. For the $\sqrt{3} \times \sqrt{3}$ cell we used the nearest equivalent k grid. Plane waves are expanded up to 60-Ry cutoff. We used a Fermi-Dirac smearing with 0.002-Ry width for B3LYP/HF/GW and a Gaussian smearing with 0.02-Ry width for LDA/GGA.

²²J. C. Slonczewski *et al.*, Phys. Rev. **109**, 272 (1958); See also Suppl. information to S. Pisana *et al.*, Nat. Mater. **6**, 198 (2007).

²³In graphite, at the high-symmetry \mathbf{H} point the four π bands are degenerate two by two, $\Delta\epsilon_0$ being the energy difference. By displacing the atoms according to the ΓE_{2g} phonon, these bands remain degenerate and the energy difference is $\Delta\epsilon$. In analogy to Eqs. (3) and (4) we define $\langle D_{\Gamma}^2 \rangle_F = (\Delta\epsilon^2 - \Delta\epsilon_0^2)/(16d^2)$. By displacing the atoms according to the $\mathbf{K} A_1'$ phonon, the four bands are no longer degenerate, being π^* (π) the two bands which are up (down) shifted and $\Delta\epsilon = \epsilon_{\pi^*} - \epsilon_{\pi}$. We define $\langle D_{\mathbf{K}}^2 \rangle_F = (\Delta\epsilon^2 - \Delta\epsilon_0^2)/(8d^2)$, where $\Delta\epsilon^2$ indicates the average between the four possible $\pi^* - \pi$ couples.

²⁴In principle, a direct calculation of $\omega_{\mathbf{K}}^{GW}$ (and thus of $B_{\mathbf{K}}^{GW}$) could be obtained, e.g., by finite differences from a prohibitively expensive GW total energy calculation.

²⁵P. Zhang *et al.*, Phys. Rev. Lett. **98**, 067005 (2007).